Journal of Colloid and Interface Science 635 (2023) 348–357

Contents lists available at ScienceDirect

Journal of Colloid and Interface Science

journal homepage: www.elsevier.com/locate/jcis

Fibrillar biocompatible colloidal gels based on cellulose nanocrystals and poly(*N*-isopropylacrylamide) for direct ink writing

Anastasia A. Belyaeva [a,b], Ilya V. Tretyakov [a], Alexey V. Kireynov [a], Yuliya A. Nashchekina [c], Vitaliy I. Solodilov [a], Evgenia G. Korzhikova-Vlakh [d], Sofia M. Morozova [a,*]

[a] *N.E. Bauman Moscow State Technical University, 2nd Baumanskaya Str,.5/1, Moscow 105005, Russia*
[b] *Institute of Physiologically Active Compounds at Federal Research Center of Problems of Chemical Physics and Medicinal Chemistry, Russian Academy of Sciences, 1 Severnij Pr., Chernogolovka, 142432 Moscow, Russia*
[c] *Institute of Cytology, Russian Academy of Sciences, Tikhoreckiy pr. 4, St. Petersburg 194064, Russia*
[d] *Institute of Macromolecular Compounds, Russian Academy of Sciences, Bolshoy pr. 31, St. Petersburg 199004, Russia*

GRAPHICAL ABSTRACT

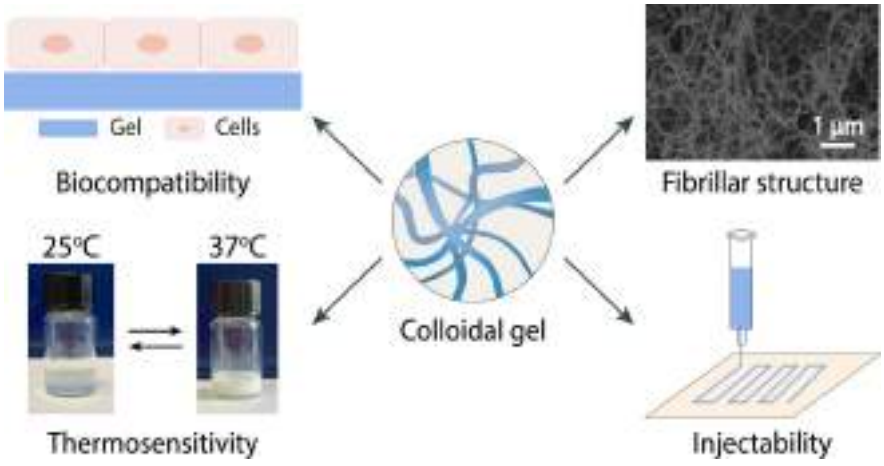

ARTICLE INFO

Article history:
Received 4 October 2022
Revised 3 December 2022
Accepted 19 December 2022
Available online 21 December 2022

Keywords:
Cellulose nanocrystals
Fibrillar gel
Colloidal gel
Shear-thinning

ABSTRACT

Hypothesis: Hydrogels based on cellulose nanocrystals (CNC) have attracted great interest because of their sustainability, biocompatibility, mechanical strength and fibrillar structure. Gelation of colloidal particles can be induced by the introduction of polymers. Existing examples include gels based on CNC and derivatives of cellulose or poly(vinyl alcohol), however, gel structure and their application for extrusion printing were not shown. Hence, we rationalize formation of colloidal gels based on mixture of poly(*N*-isopropylacrylamide) (PNIPAM) and CNC and control their structure and mechanical properties by variation of components ratio.
Experiments: State diagram for colloidal system based on mixture of PNIPAM and CNC were established at 25 and 37 °C. Biocompatibility, fiber diameter and rheological properties of the gels were studied for different PNIPAM/CNC ratio.

Abbreviations: CNC, cellulose nanocrystals; LCST, lower critical solution temperature; NPs, nanoparticles; PNIPAM, poly(N-isopropylacrylamide).

* Corresponding author at: 11th International Colloids Conference, 12-15 June 2022, Lisbon, Portugal
E-mail address: sofia.morozova@utoronto.ca (S.M. Morozova).

https://doi.org/10.1016/j.jcis.2022.12.106

Injectable hydrogel
Direct ink writing

Findings: We show that depending on the ratio between PNIPAM and CNC, colloidal system could be in sol or gel state at 25 °C and at gel state or phase separated at 37 °C. Physically crosslinked hydrogels were thermosensitive and could reversibly change it transparency from translucent to opaque in biologically relevant temperature range. These colloidal hydrogels were biocompatible, had fibrillar structure and demonstrate shear-thinning behavior, which makes them a promising material for bioapplications related to extrusion printing.

1. Introduction

Nanoparticles (NPs) are an universal building block for the formation of colloidal gels [1]. Their shape, size and nature affect on the gels' structure, mechanical, optical, transport and bioproperties [2,3]. Of particular interest is the use of anisotropic NPs, such as nanorods [4,5], nanosheets [6] or nanoplates [7], since they introduce the anisotropy of the properties to the final colloidal gel, which gives it advantages for application as actuators [4], scaffolds for cell growth [5,7,8], and sensors [9]. Among anisotropic nanoparticles, cellulose nanocrystals (CNC), has received a special prevalence due to its hydrophilicity, generally low toxicity, ability to be chemically modified in versatile fashion and cost-effectiveness [10,11 12]. In recent decades, a number of researches have focused on implantable to injectable hydrogels that enable gel formation at the desired injection site or could be 3D printed in a complex shape [13,14,15]. NP-based physical gels have thixotropic (or shear-thinning) properties, that is, they exhibit solid-like behavior at low shear and a liquid-like behavior at high shear [16]. These properties are in demand for direct ink writing and 3D extrusion printing, what inspires the design of new colloidal gels based on CNC with task-specific properties for additive technologies.

Physically crosslinked gels based on CNC can be obtained by adding salt [17], nanoparticles, [18], polymers [19,20], or grafting polymers to CNC's surface [21,22]. Among the listed strategies, gelation due to the introduction of polymers opens up the greatest opportunities for controlling the rheological and mechanical properties of the resulting material, while being one of the most cost- and time-effective in terms of the simplicity of obtaining gels. However, existing examples which include gels based on CNC and derivatives of cellulose [19,20] or poly(vinyl alcohol),[20] do not include study of gel structure and its application for extrusion printing. Moreover, an important development of the field of colloidal gels is the introduction to them of a stimuli-responsive properties, that is, the ability to undergo changes in structure–function–property relationship in response to environmental cues. Poly(*N*-isopropylacrylamide) (PNIPAM) is one of the most spread components of stimuli-responsive materials due to PNIPAM thermosensitivity related to the change in "coil-to-globule" molecular conformation above the lower critical solution temperature (LCST) in water.[23] Recent examples of obtaining physical thermosensitive gels based on PNIPAM and CNC include grafting of polymer to the CNC surface. [21,22] Such gels are in a liquid state at room temperature and transform into a gel state when the temperature rises above the LCST of PNIPAM and demonstrated promising results as cell scaffolds [21]. However, these gels required complex synthesis's strategies, purification from toxic components of polymerization catalysts and possess difficulties of precise control of molecular weight and grafting density in the case of "grafting from" approach. Also, some applications related to wound dressings, drug delivery or implants require the production of gels that maintain the gel state both below and above LCST.[24] The transition from physically crosslinked gels to covalently crosslinked ones deprives gels of thixotropic behavior and contributes to a dramatic change in gel volume during the collapse of PNIPAM above LSCT, [25] which is not always in demand, for example for wound dressings or implants. Thus, the search for new ways to obtain physically crosslinked gels based on CNC and PNIPAM is of interest for the design of 3D-printed biomaterials.

In this paper, gelation of the colloidal system based on the physical interactions between CNC and PNIPAM was investigated. The thixotropic properties of the gels were studied depending on their composition and operating temperature. We show that PNIPAM / CNC colloidal gels have fibrillar structure, thermoresponsive transparency and biocompatibility with cells. These properties of the hydrogel, along with the simplicity of its preparation, make PNIPAM / CNC hydrogel a promising platform for 3D bioprinting, cell culture, tissue engineering, wound dressings.

2. Materials and methods

2.1. Materials

Poly(*N*-isopropylacrylamide) (PNIPAM, M_n = 40,000, Sigma-Aldrich, PDI ~ 1.5), 10 wt% aqueous suspension of cellulose nanocrystals obtained by sulfuric acid hydrolysis (CNC, University of Maine Process Development), sodium hydroxide (NaOH, 98%, Sigma-Aldrich), hydrochloric acid (37% aqeous, ACS reagent), were used as received without purification.

2.2. Gel preparation

State diagram construction. Respective amount of aqueous solution of PNIPAM (19 wt%) was mixed with an aqueous dispersion of CNC (10 wt%) and water to obtain mixtures with PNIPAM/CNC = 0.5 – 4.0 (here and after we will denote this ratio as $P^{m}_{PNIPAM/CNC}$) and a total weight concentration, c_{tot}, from 4 to 16 wt % at 25 and 37 °C. Each system was stirred until a homogeneous mixture was formed (1 min). The sequence of mixing the reagents had no effect. For the state diagram at 37 °C, the samples were prepared at room temperature (otherwise PNIPAM precipitated) and heated to 37 °C using a water bath. The assignment of the resulting mixture to sol, gel or precipitate was determined visually using a flip-test.

Characterization of the gels and components by *dynamic light scattering (DLS), Fourier-transform infra-red spectroscopy (FTIR), elemental analysis, freeze drying, scanning* and *transmission electron microscopy (SEM and TEM, respectively)* and *micro computer tomography analysis* are described in Supporting Information (section S1).

Calculation of gyration radius and hydrodynamic radius. Calculations were carried out for an aqueous solution of PNIPAM, where room temperature (25 °C) is a good solvent conditions and temperature above the lowest critical dissolution temperature of PNIPAM (37 °C) is bad solvent conditions. Gyration radius was calculated for good (R_g^{25}) and poor (R_g^{37}) solvent based on equations (1) and (2), respectively [26]:

$$R_g^{25} = b^{1/5} \cdot N^{3/5} \cdot v^{2/5} \quad (1)$$

$$R_g^{37} = b^2 \cdot N^{1/3} \cdot v^{1/3} \quad (2)$$

Where b is the monomer size (0.63 nm for both 25 and 37 °C) [27], N is degree of polymerization ($N = M_n/M_{monomer}$ = 353 for both 25 and 37 °C, where M_n is molecular weight of the polymer (40,000) and $M_{monomer}$ is molecular weight of the monomer (113.16)), v is excluded volume (0.54 and 0.38 nm^3 for 25 and 37 °C, respectively) [28]. Hydrodynamic radius for good (R_h^{25}) and poor (R_h^{37}) solvent was obtained from equation (3):

$$R_h^T = R_g^T / n_T \quad (3)$$

Where n_T is ratio between experimentally determined gyration and hydrodynamic radius, the value of n_T was taken from the literature and was 1.45 and 0.77 for good and poor solvent, respectively [29].

Volume fraction ratio between PNIPAM and CNC, $P^V_{PNIPAM/CNC}$, was calculated according to eq. (4):

$$P^V_{PNIPAM/CNC} = \frac{4/3 \cdot \pi \cdot R_h^3 \cdot Ncoil}{m_{CNC} \cdot \rho_{CNC}} \quad (4)$$

Where R_h is hydrodynamic radius at respective conditions (bad or poor solvent), N_{coil} is amount of PNIPAM coils in the mixture defined as $N_{coil} = N_A \cdot m_{PNIPAM}/M_n$ (where N_A is Avogadro number, m_{PNIPAM} is mass of PNIPAM in the mixture), m_{CNC} is mass of the CNC in the mixture and ρ_{CNC} is the CNC's density, 1.5 g/cm^3 [12].

Amount of PNIPAM coils per one CNC, $P^N_{PNIPAM/CNC}$, was calculated according to eq. (5):

$$P^N_{PNIPAM/CNC} = \frac{Ncoil}{N_{CNC}} \quad (5)$$

Where N_{CNC} is amount of CNC particles in the mixture and defined as $N_{CNC} = m_{CNC}/m_{1\text{-}CNC}$, and $m_{1\text{-}CNC}$ is mass of 1 CNC particle, i.e $m_{1\text{-}CNC} = \rho_{CNC}\, \pi \cdot R_{CNC} \cdot L_{CNC}$ (R_{CNC} is CNC radius, 8.3 ± 1.9 nm, and L_{CNC} is CNC length, 151 ± 54 nm).

Amount of PNIPAM coils per one CNC by surface area, $S^T_{PNIPAM/CNC}$, was calculated at certain T according to eq. (6):

$$S^T_{PNIPAM/CNC} = \frac{S_{1-CNC}}{S_{1-PNIPAM}} \quad (6)$$

Where S_{1-CNC} is surface area of one CNC particles in the mixture and defined as $S_{(1-CNC)} = 2 \cdot \pi \cdot R_{CNC} \cdot L_{CNC} + 2 \cdot \pi \cdot R^2_{CNC}$, and $S_{1-PNIPAM}$ is the surface area of the largest cross-section (diameter) of 1 PNIPAM coil , i.e $S_{1-PNIPAM} = \pi \cdot R_h^2$.

Rheology experiments. Rheology measurements was performed using an Anton Paar MCR 702 (Austria) rheometer with cone (diameter 25 mm) and plate geometry, and a gap of 108 μm at temperature 25 °C and 37 °C. To control the temperature, an integrated Peltier plate were used. To measure the viscosity at different shear rates and storage modules, the systems were equilibrated for 15 min at certain temperature (25 or 37 °C). Studies in the oscillatory mode were carried out at a frequency of 10 rad/s. The shear modulus G' and the loss modulus G'' were recorded over time (strain 1 %) and with a change in displacement (strain) from 0.1 to 30 %. Studies in the rotational mode were carried out in the range of shear rates from 0.1 to 30 s^{-1} to determine the dynamic (shear) viscosity η. The recovery of the system after the application of shear stress was carried by determination of the dynamic viscosity at a shear rate of 0.1 s^{-1} for 500 s and 40 s^{-1} for 500 s. Then the cycle was repeated one more time.

Ink preparation. Ink for printing with a c_{tot} of 13.0 wt% and a$P^m_{PNIPAM/CNC}$ = 1 was prepared by mixing 500 mg 10 wt% CNC (aq) and 260 μL 19 wt% PNIPAM (aq). Bromophenol blue food dye (0.02 g per 5 ml of gel) was added to the resulted ink to visualize the injectability of the gel.

Direct ink writing. Inks with a c_{tot} of 13.0 wt% and a$P^m_{PNIPAM/CNC}$ = 1 was placed in syringe with needle 22G and manually extruded on a glass substrate at r.t. (25 °C). Extruded pattern was placed at heating plate at 37 °C for 10 min, and then cooled down to r.t. at ambient conditions. Four cycles of heating–cooling were repeated.

Biological evaluation. In vitro biocompatibility of the gels was examined using the human epidermal cell line (A-431). The cell line was obtained from the Cell Culture Collection of the Institute of Cytology RAS (St. Petersburg, Russia). The cells were cultured in polystyrene flasks in DMEM supplemented with 10 % FBS, 1 % penicillin/streptomycin (Sigma-Aldrich, Darmstadt, Germany) at 37 °C in a humidified atmosphere of 5 % CO_2 in air. Subconfluent cells were passaged by using trypsin– EDTA (0.25 % (*w*/*v*) trypsin, 1 mM EDTA). The samples of the gels were injected into the wells of 96-well plate at a volume of 60 μL/well (n = 3 for each gel composition) and incubated at room temperature with an orbital shaking until the gel was evenly distributed on the surface. Before cell seeding, the plate was incubated at 37 °C for 5 min. Then, 100 μL of medium with 1×10^4 cells were added to each test sample and incubated at 37 °C with 5 % CO_2 for 72 h. The wells of the plate (n = 3) were used as a control surface. The cell viability was evaluated with the use of standard MTT assay as described elsewhere [30]. Bright-filed optical microscopy of cells was performed using a Nikon Eclipse TS100 microscope with a color digital camera (×10). For this purpose, cells were cultivated in the same way as described above, but in a 24-well plate (350 μL of gel/well).

3. Results and discussion

3.1. Gel formation

Gelation of an aqueous dispersion of anisotropic rod-shape NPs (CNC), and an aqueous solution of thermoresponsive polymer (PNIPAM), was studied in the ratios of components of mass ratio PNIPAM / CNC = 0.5 – 4.0 (here and after we will denote mass ratio as $P^m_{PNIPAM/CNC}$) and a total weight concentration, c_{tot}, from 4 to 16 wt%. The dimension of CNC was calculated from TEM images: length was 151 ± 54 nm, diameter was 16 ± 4 nm (Fig. S1a,b, Supporting information). Colloidal stability of CNC is caused by half-ester -SO_3H groups and concentration of these groups was estimated as 0.32 mmol·g^{-1} based on the sulfur content 1.03 wt%. The resulting colloidal gels was formed due to depletion forces related with charge screening of CNC by PNIPAM coils, acting as a depletant [31,32]. Adsorption of PNIPAM on CNC surface was achieved due to physical interactions, namely the formation of hydrogen bonds between —OH and —SO_3H groups of CNC and —NH and —C=O groups of PNIPAM, as well as hydrophobic interactions (Fig. 1a, Fig. S2, Supporting Information). By variation of $P^m_{PNIPAM/CNC}$ and c_{tot}, state diagram for colloidal system PNIPAM / CNC was obtained at room temperature (25 °C) and 37 °C (Fig. 1b,c). At 25 °C gel was formed at c_{tot} > 8 wt% and $P^m_{PNIPAM/CNC}$ from 0.5 to 1.7 (Fig. 1b, gel region), while for the remaining ratios the system appeared as homogeneous translucent liquid (Fig. 1b, sol region).

Next, we investigated the phase behavior of the system at a temperature above LCST (~32 °C) of PNIPAM [29]. We chose 37 °C as the operating temperature, which satisfies the criterion $T > T_{LCST}$ and coincides to the biological temperature of tissues. At 37 °C regions which at 25 °C were in sol state (for the $P^m_{PNIPAM/CNC}$ > 2) phase separated into a translucent dispersion and a white precipitate, while those regions which at 25 °C were in a

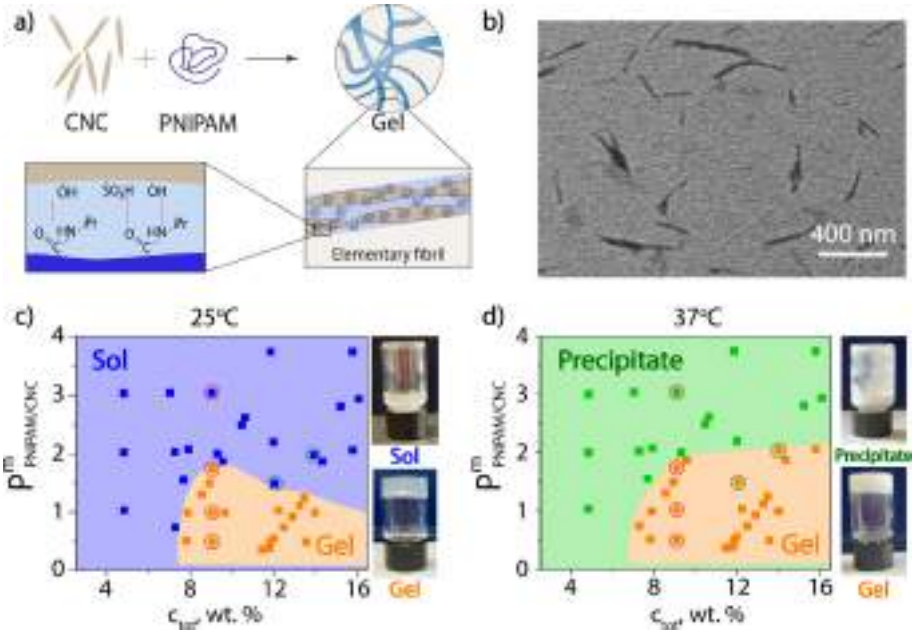

Fig. 1. a) scheme of colloidal gel formation from aqueous dispersion of CNC and aqueous solution of PNIPAM; b) TEM image of CNC demonstrating rod-like structure of nanoparticles; c-d) state diagram for aqueous dispersion of CNC and PNIPAM at 25 °C (c) and 37 °C (d). Points for which rheology was investigated further are marked with orange circles, while points that are a gel at 37 °C and a sol at 25 °C are marked with green circles.

gel state remained in the gel state but became opaque (Fig. 1c). Precipitation occurs due to insolubility of PNIPAM above LCST and has reversible nature (Fig. S3, Supporting information).

Interestingly, compositions, namely, c_{tot} = 14 wt%, $P^m_{PNIPAM/CNC}$ = 2.0 and c_{tot} = 12 wt%, $P^m_{PNIPAM/CNC}$ = 1.5, which were in a liquid state at 25 °C, formed a gel at 37 °C (Fig. 1c,d marked with green circles). The size of the CNC, as well as its zeta potential, does not change during the temperature transition from 25 to 37 °C (Fig. S3a,b, Supporting information). We associate this with the change in volume ratio of PNIPAM / CNC, $P^V_{PNIPAM/CNC}$, due to "coil-to-globule" transition of PNIPAM above LCST. This transition led to dramatic change of gyration radius of PNIPAM, R^T_g, from 24.2 nm for good solvent (water at 25 °C) to 4.1 nm for poor solvent (water at 37 °C) and change in R^T_h, from 16.7 nm for good solvent (water at 25 °C) to 5.4 nm for poor solvent (water at 37 °C). Experimental values obtained by DLS for R_h were slightly higher then calculated one and were 21 and 8 nm at 25 and 37 °C, respectively (Fig. S4a, Supporting Information). Table 1 shows the difference in volume, mass, surface area and particle number ratios for $P_{PNIPAM/CNC}$ at 25 and 37 °C.

It was previously shown that the topology of the phase diagram of colloidal NPs and linear polymer is determined by the size ratio, ψ, where $\psi = R_g/R_{NPs}$ (R_{NPs} is the radius of colloidal particles ($R_{NPs} = L/2$ for CNC)). For ψ < 0.25 the addition of the polymer simply expands the colloidal fluid-crystal coexistence region, while for $\psi \geq 0.25$ a three-phase coexistence of colloidal gas, liquid, and crystal phases could be observed. [32,33]. For a system in condition of a good solvent (25 °C) ψ = 0.32 > 0.25, i.e., colloidal gas, liquid, and crystal phases coexistence in the system. This can also be concluded by comparing the volume ratio, $P^V_{PNIPAM/CNC}$, and the number of PNIPAM coils per 1 CNC at the maximum filling area of the particle surface, $S_{PNIPAM/CNC}$. For samples S1-S4 (Table 1) at 25 °C with the same total concentration (c_{tot} = 9 wt%), but a different ratio of $P^m_{PNIPAM/CNC}$ changing from 3 to 0.5, the $P^V_{PNIPAM/CNC}$ changing from 1325 to 221, respectively, while maximum filling of the surface of 1 CNC corresponds to $S_{PNIPAM/CNC} = 20$ polymer coils (excluding deformation during adsorption). Number particle ratio $P^N_{PNIPAM/CNC}$ for samples S1-S4 is changing from 2201 to 367, which is also much higher that $S_{PNIPAM/CNC} = 20$. Thus, at good solvent conditions a large excess of polymer may be expected, and it could be in the colloid-poor phase, i.e. there is a colloidal gas or liquid. For poor solvent conditions ψ = 0.05 < 0.25, which is case of transition from fluid to classical depletion colloidal gel depending on polymer concentration [34]. For samples S1-S4 at 37 °C $S_{PNIPAM/CNC} = 194$ which is higher then $P^V_{PNIPAM/CNC}$ ranging from 44 to 7. Thus, for each condition (both at 25 and at 37 °C), there are optimal polymer-NPs ratios leading to gel formation. A similar "liquid-gel-liquid" transi-

Table 1
Volume, mass, surface area and particle number ratio between PNIPAM and CNC at good solvent conditions (25 °C) and poor solvent conditions (37 °C).

Sample	c_{tot}, wt.%	$P^m_{PNIPAM/CNC}$	$P^N_{PNIPAM/CNC}$	$P^V_{PNIPAM/CNC}$		ψ		$S_{PNIPAM/CNC}$		State of the system	
				25 °C	37 °C	25 °C	37 °C	25 °C	37 °C	25 °C	37 °C
S-1	9	3.0	2201	1325	44	0.32	0.05	20	194	sol	precipitate
S-2	9	1.7	1247	751	25					gel	gel
S-3	9	1.0	734	442	15					gel	gel
S-4	9	0.5	367	221	7					gel	gel
S-5	14	2.0	1467	884	30					sol	gel

c_{tot} - total weight concentration; $P^m_{PNIPAM/CNC}$ - mass ratio (dimensionless); $P^N_{PNIPAM/CNC}$ - ratio between PNIPAM coils and CNC particles (dimensionless); $P^V_{PNIPAM/CNC}$ - volume ratio (dimensionless); ψ - size ratio (dimensionless); $S_{PNIPAM/CNC}$ - maximum filling area of the particle surface (dimensionless).

tion with a change in the depletant-nanoparticle ratio was also observed earlier for a system based on polystyrene spheres as NPs and PNIPAM microgels as depletants [35]. Comparison of samples S1 and S5 (Table 1) shows that their volume ratios, 1325 and 884, respectively, are outside the gel zone for 25 °C, while for 37 °C, sample S1 volume fraction $P^{V}_{PNIPAM/CNC}$ = 44, remains outside the gel region for 37 °C and is phase separated, and sample S5 turns into a gel with $P^{V}_{PNIPAM/CNC}$ = 30. Considering the nature of depleted forces (osmotic pressure created by polymer tangles (depletants) bringing particles closer together) [36], it is expected that the interaction between CNC in the gel under poor solvent conditions will be stronger than the same under good solvent conditions.

3.2. Gel structure

Due to the anisotropic shape of the CNC, the gels formed on its basis have a fibrillar structure [1,2], (Fig. 2a-d) while pure polymer have no defined structure (Fig. 2e).

It was previously demonstrated that fibrillar gels could be formed by physical crosslinking of CNC caused by salt addition [17]. Here we use depletion forces originated from PNIPAM to form gel. Based on the literature fibrillar structure for gels based on covalently crosslinked CNC and polymer could be achieved for ratios $P^{m}_{PNIPAM/CNC}$ < 10 [5]. Thus, our gels are physically crosslinked by depletion forces and the ratio between CNC and polymer are in the range of fibrillar structure 0.5 < $P^{m}_{PNIPAM/CNC}$ < 1.7. We show that by changing $P^{m}_{PNIPAM/CNC}$ it is possible to obtain fibrils with different diameters (Fig. 2a-c), which is in agreement with previously reported data for gels formed form CNC covalently grafted with polymer [5]. With a decrease of $P^{m}_{PNIPAM/CNC}$ from 1.7 to 0.5 the diameter of the fibrils decreases from 38 to 30 nm (Fig. 2a-c). The diameter of fibrils of the salt-induced CNC gel (Fig. 2d) was 30 nm, which is equal to two CNC diameters (R_{CNC} = 8.3 ± 1.9 nm based on TEM analysis, Fig. S1a,b, Supporting Information). Monotonic increase in the diameter of the fibrils with an increase of the concentration of PNIPAM is associated with the adsorption of a polymer on the surface of fibrils. The values of the diameter of the fibrils at 37 °C coincide with the values at 25° C within the margin of error (Figure S5, Supporting information).

The fibrillar structure on the nanoscale level leads to the layer structure of the resulting gel on the microscopic level (Fig. 2g,h). According to the tomography data gels have porous structure with a total volume pore space, V_p, for 25 and 37 °C were 0.37·and 0.17 mm^3. The total porosity for gels were 74 and 73 % for 25 and 37 °C, respectively. Thus, structure of gels at 25 and 37 °C was similar both on nano- and microscale levels.

3.3. Thermosensitive behavior and pH effect

It is well known that PNIPAM-based gels are thermosensitive, due to the "coil-to-globule" transition of PNIPAM in water at temperatures above the LCST [37]. The gels obtained in this work process thermal sensitivity, which was expressed in a change in transparency from translucent at T < T_{LCST} (Fig. 3a top) to opaque at T>T_{LSCT} (Fig. 3a bottom). The translucency of the gels was the same for compositions with different total concentrations (Fig. S6, Supporting Information).

It is important to note that the thermal transition did not affect on the total volume of the gel, unlike gels based on covalently crosslinked PNIPAM (Fig. 3a), which collapse with a dramatic decrease in volume [38,39]. Volume retention is promising for extrusion printing and some biomedical applications, such as wound dressings or implants.

Fig. 3b demonstrated dependence of thermosensitive properties of the gels with same total concentration 9 wt%, but differ in their compositions, namely, $P^{m}_{PNIPAM/CNC}$ equal to 1.7, 1 and 0.5. We found that with decreasing $P^{m}_{PNIPAM/CNC}$ from 1.7 to 0.5 lead to the increase of LCST temperature of the gel in comparison with the pure PNIPAM from 31 to 36 °C (Fig. 3c). This is in the agreement with liter-

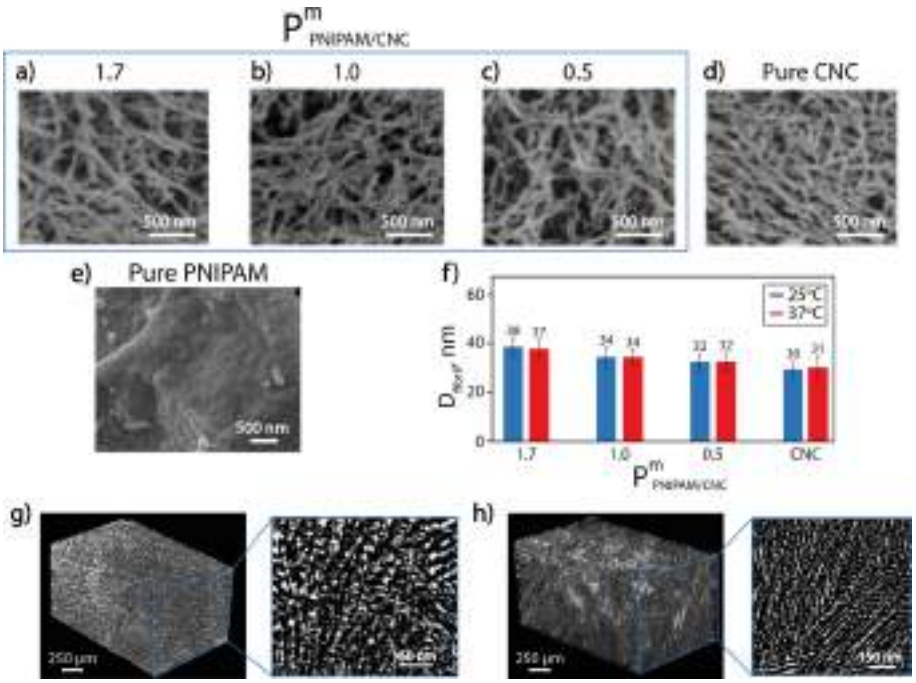

Fig. 2. a)-c) SEM images of gels incubated at 25 °C with c_{tot} = 9 wt% and different ratios of PNIPAM and CNC: $P^{m}_{PNIPAM/CNC}$ = 1.7 (a), $P^{m}_{PNIPAM/CNC}$ = 1.0 (b) and $P^{m}_{PNIPAM/CNC}$ = 0.5 (c); d) SEM image of gel obtained by slat-induced gelation of CNC; e) SEM image of a dried PNIPAM; f) average diameter of the fibrils for different ratios of $P^{m}_{PNIPAM/CNC}$ calculated based on SEM images; g-h) images of the structure of gel with c_{tot} = 13 wt% and a mass ratio $P^{m}_{PNIPAM/CNC}$ = 1.0 obtained by X-ray microtomography at 25 °C (g) and 37 °C (h).

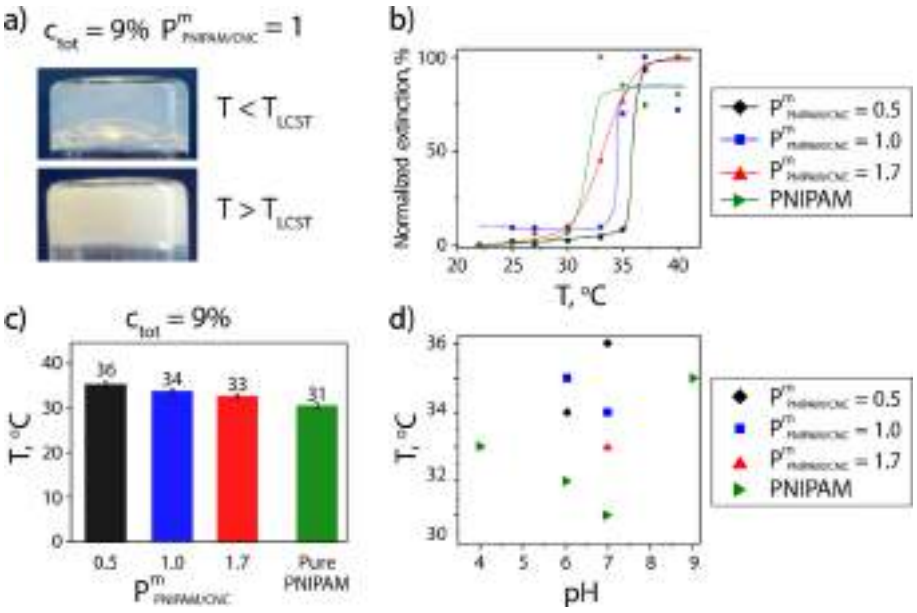

Fig. 3. Effect of gel's composition on its LCST. a) appearance of the gel c_{tot} = 9 wt% and$P^m_{PNIPAM/CNC}$ = 1 below (25 °C) and above (37 °C) LCST; b) temporal variation in the normalized extinction of the gels with total concentration 9 wt% and different ratios of PNIPAM and CNC, namely, $P^m_{PNIPAM/CNC}$equal to 1.7, 1 and 0.5. The solid lines are given for eye guidance; c) LSCT values of PNIPAM solution and gels with total concentration 9 wt% and $P^m_{PNIPAM/CNC}$equal to 1.7, 1 and 0.5; d) effect of pH on the gels' and PNIPAM LCST. Data are provided only for system which were stable at certain pH.

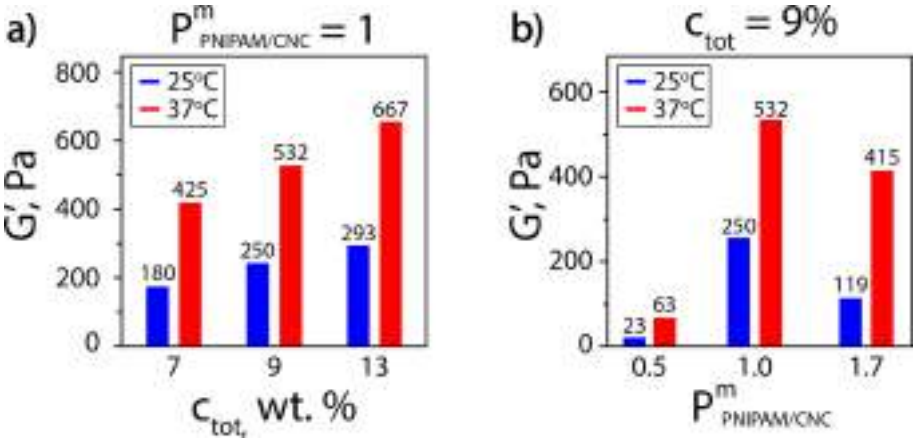

Fig. 4. a) dependence of the values of the storage modulus G' for gels with the same $P^m_{PNIPAM/CNC}$ = 1 and different c_{tot}; b) dependence of the values of the storage modulus G' for gels with the same c_{tot} = 9 wt% and different $P^m_{PNIPAM/CNC}$.

ature data and explained by the change of the gel's hydrophilic / hydrophobic balance: with decreasing $P^m_{PNIPAM/CNC}$ the concentration of CNCs increase (and hence, hydrophilic –OH and -SO_3H groups) made the environment of PNIPAM more hydrophilic and thus increased its LSCT [25,40,41]. Thus, the transition temperature (LCST) can be varied by changing the composition of the gel in biologically relevant region.

Next, we investigate the effect of pH on the gel stability for gels with total concentration 9 wt% and $P^m_{PNIPAM/CNC}$ equal to 1.7, 1 and 0.5 (Fig. 3d). All gels have initially pH 7, because of initial components, CNC aqeous dispersion and PNIPAM aqeous solution, has pH 7. We found that all gels become unstable at basic pH $\geq$ 8 and at acidic pH 4. At slightly acidic pH 6 gels with $P^m_{PNIPAM/CNC}$ equal 1 and 0.5 were stable, while gel with $P^m_{PNIPAM/CNC}$ equal to 1.7 precipitated (Table S1, Supporting Information). The effect of pH was attributed to the change of zeta-potential of CNC: when pH was differed from 7, zeta potential increase from −44 mV to –23 mV (Fig. S6a, supporting information) which is in the agreement with previously reported data [42,43]. Thus, instability of the gels could be explained by reduced colloidal stability of CNC. Change in pH from 7 to 6 has insignificant effect on the gel's LCST (Fig. S7b, Table S1, Supporting Information).

3.4. Rheological properties

Rheological properties of the hydrogels were investigated depending on the total concentration and ratios of PNIPAM and CNC. For the ratio $P^m_{PNIPAM/CNC}$ = 1 when the c_{tot} of the components increases from 7 to 13 wt%, the shear modulus G' changes at 25 °C from 180 to 293 Pa (Fig. 4a).

This data are in the agreement with the previously reported data for systems based on polymer-CNC mixture, i.e. CNC has a reinforcing effect on the polymer gels [19]. The significant increase in the shear modulus by 2.1–2.4 times at 37 °C was associated with

a more pronounced contribution of depletion forces, due to a change in the scale ratio ψ and the volume fraction of the polymer, which led to reducing the coverage of the surface of the particles [44]. Values of *G'* at 37 °C range from 425 to 667 Pa for the ratio $P^{m}_{PNIPAM/CNC}$ = 1 with an increase in c_{tot} from 7 to 13 wt%, respectively (Fig. 4a).

Mechanical properties alter non-monotonically when the ratio of $P^{m}_{PNIPAM/CNC}$ = 0.5 – 1.7 components changed (Fig. 4b, Fig. S9 Supporting Information). For the c_{tot} = 9 wt%, the highest value of the strength modulus *G'* was achieved with the ratio$P^{m}_{PNIPAM/CNC}$ = 1 and is 250 Pa at 25 °C ($P^{V}_{PNIPAM/CNC}$ = 442), and 540 Pa at 37 °C ($P^{V}_{PNIPAM/CNC}$ = 14). With the ratio$P^{m}_{PNIPAM/CNC}$ = 0.5 *G'* is 23 Pa at 25 °C ($P^{V}_{PNIPAM/CNC}$ = 221), and 63 Pa at 37 °C ($P^{V}_{PNIPAM/CNC}$ = 7). And with the ratio $P^{m}_{PNIPAM/CNC}$ = 1.7 *G'* is 119 Pa at 25 °C ($P^{V}_{PNIPAM/CNC}$ = 751), and 415 Pa at 37 °C ($P^{V}_{PNIPAM/CNC}$ = 25). When switching from $P^{m}_{PNIPAM/CNC}$ = 1 to$P^{m}_{PNIPAM/CNC}$ = 1.7 there is a 2.1-fold decrease in *G'* for 25 °C and 1.3-fold for 37 °C. The higher the content of PNIPAM in the system, the higher the difference for *G'* for 25 °C and 37 °C (119 and 415) and (23 and 63) by 3.5 times, and 2.7 times, respectively. As a control experiment, we investigated the rheological properties separately only of the PNIPAM solution and separately only of the CNC aqueous dispersion. Concentrations equivalent to the concentrations of the corresponding components in the gel were selected. It is shown that at 25 °C both PNIPAM and CNC demonstrate liquid behavior, i.e. $G' < G''$ (Table S2, Fig. S8a,c), while their mixture is a gel. At 37 °C, the CNC exhibits fluid behavior, i.e. $G' < G''$ (Table S2, Fig. S8b, Supporting Information), and PNIPAM precipitates (Fig. S8d, Supporting Information), their mixture is a gel. This nonmonotonic dependence is determined by the existence of optimal ratios of PNIPAM and CNC in the gelation region, which will lead to the presence of a region of maximum contribution of depleted forces.

Due to the fact that the gels are formed through physical interactions (depletion forces and hydrogen bonding), they demonstrate thixotropic properties, i.e. a decrease in viscosity with an increase in shear rate, which is highly beneficial for the application of gels as inks for direct ink writing or extrusion based 3D printing [1]. Gel with c_{tot} = 13 wt%, $P^{m}_{PNIPAM/CNC}$ = 1 was selected as ink since it has the highest values of the *G'* among other compositions with a different mass fraction and other ratios. The *G'* increases from 293 Pa to 667 Pa when the temperature rises from 25 to 37 °C (Fig. 5a).

When the strain reaches > 21 % (Fig. 5b), the gel is destroyed ($G''/G' < 1$) at 25 °C, and at 37 °C the maximum strain required for the destruction of the gel increases to 42 %. This indicates an increase in the strength of the gel at a higher temperature associated with an increase in the contribution of depletion forces, which was described in Section 3.1.

The shear-thinning behavior of the gel was confirmed by rheological studies of shear viscosity, η, at different shear rates, $\dot{\gamma}$, (Fig. 5c). At $\dot{\gamma}$ = 0.1 s^{-1}, the viscosity was 400 and 1000 Pa·s for 25 and 37 °C, respectively, and at $\dot{\gamma}$ = 30 s^{-1}, the viscosity decreased to 2 and 5 Pa·s for 25 and 37 °C, respectively. Next, we studied the recovery of η upon cyclic change of $\dot{\gamma}$ from 0.1 to 40 s^{-1}, that is, the "self-healing" properties of the colloidal gel which determine its ability to preserve its shape after shear-stress or extrusion (Fig. 5d). At 25 and 37 °C, a periodic step-wise change in $\dot{\gamma}$ in the range from 0.1 to 40 s^{-1} led to a change in the shear viscosity of the gel. At 25 °C and an initial value of $\dot{\gamma}$ = 0.1 s^{-1}, the value of η was 25 ± 3 Pa·s, an increase of $\dot{\gamma}$ up to 40 s^{-1}, lead to the decrease in η by 29 times. Subsequent decrease of $\dot{\gamma}$ to 0.1 s^{-1} led to an increase in η to 26 ± 2 Pa·s, that is, to the recovery of almost 100 % of the original value of η. At 37 °C and the initial value of$\dot{\gamma}$ = 0.1 s^{-1}, the value of η = 290 ± 180 Pa·s, an increase in $\dot{\gamma}$ to 40 s^{-1} led to a decrease in η by 152 times. The subsequent decrease of $\dot{\gamma}$ to 0.1 s^{-1} led to an increase in η to 160 ± 40 Pa·s, that is, to the restoration of 55 % of the original value of η. Thus, the ink has rheological properties that can be used for extrusion printing: liquefaction during shear and rapid recovery of ink viscosity after reducing the shear stress. Printing at 25 °C is more beneficial than printing at 37 °C due to higher recovery of the inks.

3.5. In vitro biocompatibility

The evaluation of the *in vitro* biocompatibility of gel samples was carried out using A-431 cells. For this purpose, cells were seeded on the surface of gel coats previously created at the bottom of the plate wells. The non-covered bottom of wells was used as a control surface. The seeded cells were incubated for 72 h at 37 °C, and after that the cell proliferation was examined by MTT assay. The results, presented in Fig. 6a, demonstrate the high biocompatibility of the cells with gel matrices. The higher optical density of formazan in the case of tested gels means the higher number of living cells compared to control (metabolic activity was about 200 % and more with respect to control). This result is explained by the difference in the space available for cell growth: the control surface is two-dimensional (2D), while the gel coats have a three-dimensional (3D) space. In turn, this leads to a faster confluence of cells on the 2D surface in contrast to the gels. Thus, active cell proliferation and high viability of cells after 3 days indicate a cell friendly environment providing by the PNIPAM / CNC gels. At the same time, there were no drastic differences in cell viability depending on the gel composition.

In addition, to confirm our assumption about the positive effect of the gel on cell support and growth in the gel space, we examined the control and gel surfaces by bright-field optical microscopy (Fig. 6b-d). A-431 cells in the control (the bottom of cell culture plate) after 72 h of cultivation have a typical shape for epithelial cells, attached to the surface of the culture plate. However, in some cells, one can observe outgrowths or phyllapodia not characteristic to epidermal cells. Such phenomena in the morphology of cells can be attributed to the peculiarities of cultivation on the culture plate. In turn, no such phyllopodia were observed when cells were cultured on gels. All cells had a typical shape. The softness of the gel promotes partial immersion of cells in the gel. It should also be noted that after 72 h of cultivation, the number of cells on the gel surfaces exceeded the number of cells in the control sample. The obtained result is in complete agreement with the MTT-analysis data discussed above.

3.6. Direct ink writing (injectability) with PNIPAM / CNC inks

Chosen composition of colloidal gel, with c_{tot} = 13 wt%, $P^{m}_{PNIPAM/CNC}$ = 1, was tested for direct ink writing using a syringe with 22G needle at 25 °C. The choice of the $P^{m}_{PNIPAM/CNC}$ ratio was explained by its highest biocompatibility and highest storage modulus among other ratios. Fig. 7a shows that the developed ink was squeezed out as a continuous homogeneous filament at 25 °C (dye was used to increase contrast between the filament and the aqueous medium).

To utilize the shear-thinning behavior of the obtained inks, we examined the hydrogel performance as an injectable material by manual extrusion from the syringe on a horizontal glass slide surface to produce logo of the university (Fig. 7b). Upon extrusion, the hydrogel retained its threadlike shape and formed a predesigned pattern, which prove shear-thinning properties of the developed inks (Fig. 7b). Extruded pattern was translucent at 25 °C (Fig. 7b)

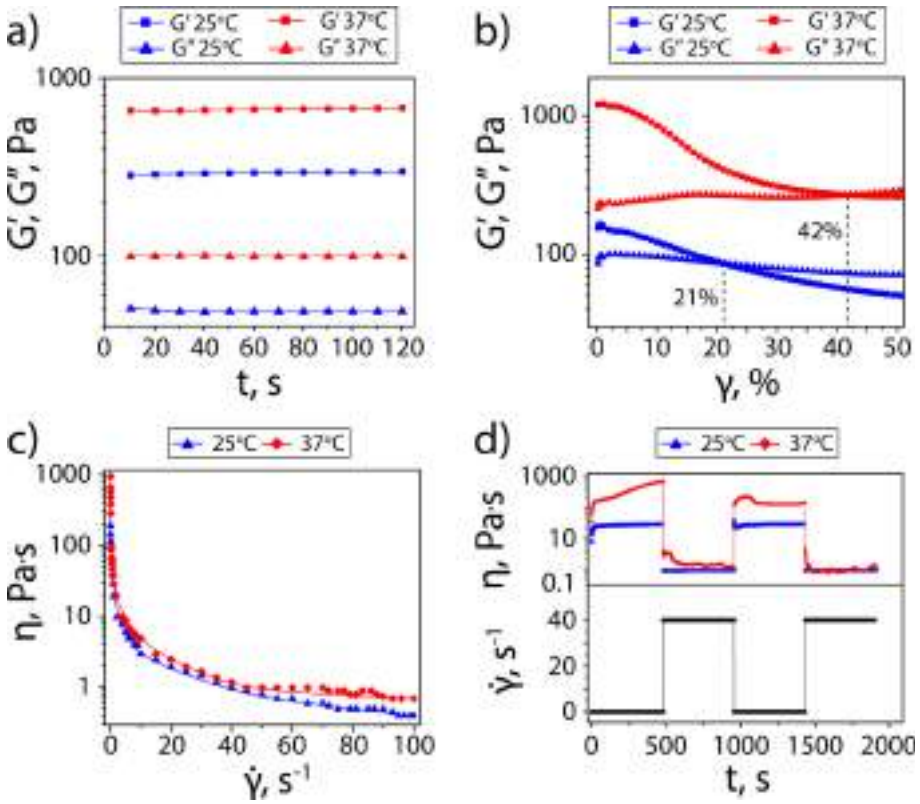

Fig. 5. Rheological properties of gel a c_{tot} = 13.0 wt% and $P^{m}_{PNIPAM/CNC}$ = 1. a) Time-dependency of storage modulus G' and loss modulus G'' at strain 1 % and 10 rad/s; b) Variation storage modulus G' and loss modulus G'' of the gel, plotted as a function of the shear strain γ; c) Variation in shear viscosity η of the gel, plotted as a function of the shear rate $\dot{\gamma}$; d) Time-dependent variation in shear viscosity η of gel (top) at corresponding variation of $\dot{\gamma}$ (bottom).

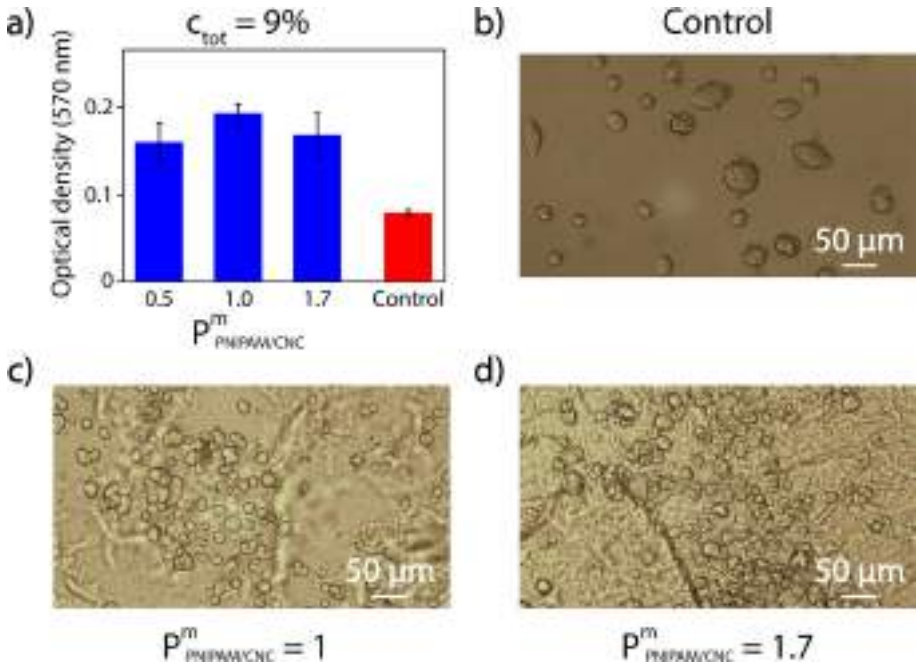

Fig. 6. a) proliferation of a-431 cells on the control surface (bottom of the wells of the adhesion cell culture 96-well plate) and the surface of gels with the same c_{tot} = 9 wt% and different $P^{m}_{PNIPAM/CNC}$ (MTT assay, 72 h). b)-d) Bright-field optical microscopy (×10) of A-431 cells on the control surface (bottom of the adhesion cell culture 24-well plate) (b) and the surface of gels with the same c_{tot} = 9 wt% and different $P^{m}_{PNIPAM/CNC}$: 1.0 (c) and 1.7 (d).

and becomes non-transparent (opaque) when heated up to 37 °C (Fig. 7c). It has been shown that the transition of the gel pattern from a transparent to a non-transparent state is completely reversible within 4 cycles (Fig. S11, Supporting Information, video s1). The resulting gels could form translucent brittle films upon drying (Fig. S9, Supporting Information). Further cycling was accompanied

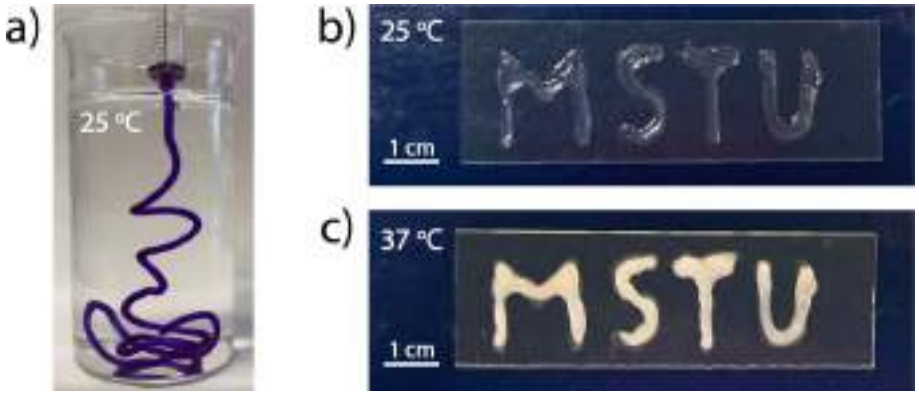

Fig. 7. a) extrusion of a gel sample at 25 °C (bromophenol blue dye was added for achievement of a higher contrast in the aqueous media); b) logo of the university obtained by direct ink writing with ink c_{tot} = 13 wt%, $P^{m}_{PNIPAM/CNC}$ = 1 (ink temperature 25 °C) on the glass substrate at 25 °C; c) logo of the university obtained by direct ink writing with ink c_{tot} = 13 wt%, $P^{m}_{PNIPAM/CNC}$ = 1 (ink temperature 25 °C) on the glass substrate at 37 °C;

with a significant drying of the gel. The extruded pattern retains its shape during the heating–cooling cycles since the ink composition was selected according to the state diagrams to be gel at both 25 °C (Fig. 1c) and 37 °C (Fig. 1d). However, it is possible to select compositions when the system is in a gel state at 37 °C and liquefies at 25 °C.

4. Conclusion

On the basis of previously reported approaches for non-stimuli responsive polymers [45,46] we developed an injectable fibrillar colloidal hydrogel formed from anisotropic rod-like cellulose nanocrystals and thermosensitive poly(*N*-isopropylacryalmide). The hydrogel formed as a result of the attractive depletion forces created by polymer coils which overcame the electrostatic repulsion between the negatively charged half-ester sulfate groups of CNC and hydrogen bonds between —OH and —SO_3H groups of CNC particles and —NH and —C=O groups of PNIPAM. Although physically crosslinked gels based on CNC and polymer were previously reported,[45,46] their fibrillar structure and its features such as the diameter of the fibrils depending on the gel's components and temperature, were demonstrated by us for the first time. The resulting gel possess stimuli-responsive properties: a) for all gel compositions, a change in transparency from translucent to opaque was observed during the transition from 25 to 37 °C, and b) for some compositions (c_{tot} > 10.0 wt% and a mass ratio $P^{m}_{PNIPAM/CNC}$ > 1.3), the gelation was temperature induced and systems were in a sol state at 25 °C and in a gel state at 37 °C and c) for compositions that were gels at both 25 and 37 °C, the temperature transition is accompanied by an increase in mechanical properties (the storage modulus increases by 2–3 times). Moreover, it was shown that the transition temperature can be adjusted in biologically relevant range from 33 to 36 °C by changing the ratio of PNIPAM and CNC.

In contrast to the previously reported gels based on PNIPAM grafted to CNC,[47,21,48] gels developed in this work demonstrated shear-thinning behavior without temperature change and could be printed at either 25 or at 37 °C. The resulting hydrogels were biocompatible, exhibited shear-thinning behavior and their mechanical properties as well as temperature sensivity could be tuned by varying the PNIPAM and CNC concentrations. We demonstrated that hydrogel was suitable as an injectable material for direct ink writing. Thus, developed colloidal gels can be a simple and convenient platform for bioapplications, where further development of the work may be associated with introduction to the gel task-specific properties. For example, the adsorption of hydrophilic therapeutic agents at 25 °C (when PNIPAM is in a hydrophilic state) and their release by the "squeezing out" mechanism [24,49] at 37 °C due to the collapse of PNIPAM. Another promising direction is the application of developed gel as bioink for extrusion printing implants by incorporation of cells in the gel's structure. [50].

CRediT authorship contribution statement

Anastasia A. Belyaeva: Conceptualization, Writing – original draft, Data curation, Methodology, Investigation. **Ilya V. Tretyakov:** Investigation. **Alexey V. Kireynov:** Investigation, Methodology. **Yuliya A. Nashchekina:** Investigation, Methodology. **Vitaliy I. Solodilov:** Formal analysis, Validation, Writing – review & editing. **Evgenia G. Korzhikova-Vlakh:** Conceptualization, Validation, Data curation, Writing – review & editing. **Sofia M. Morozova:** Project administration, Conceptualization, Writing – original draft, Supervision, Funding acquisition.

Data availability

Data will be made available on request.

Declaration of Competing Interest

The authors declare that they have no known competing financial interests or personal relationships that could have appeared to influence the work reported in this paper.

Acknowledgments

This work was performed with the financial support from the grant of Russian Science Foundation (Project No. 21-79-20113). This work was in part carried out using equipment of the SPbU Resource Centers and center of national technology initiative "Digital materials science: new materials and substances" (rheological studies).

Appendix A. Supplementary material

Supplementary data to this article can be found online at https://doi.org/10.1016/j.jcis.2022.12.106.

References

[1] Y, Zeng, M, Zhang, Colloidal nanoparticle inks for printing functional devices: Emerging trends and future prospects, J. Mater. Chem. A. 7 (2019) 23301–23336. https://doi.org/10.1039/C9TA07552F.

[2] S.M. Morozova, T.G. Statsenko, E.O. Ryabchenko, A. Gevorkian, V. Adibnia, M.S. Lozhkin, A.V. Kireynov, E. Kumacheva, Multicolored Nanocolloidal Hydrogel Inks, Adv. Funct. Mater. 2105470 (2021) 1–8, https://doi.org/10.1002/adfm.202105470.
[3] P. Zarrintaj, A.M. Urbanska, S.S. Gholizadeh, V. Goodarzi, M.R. Saeb, M. Mozafari, A facile route to the synthesis of anilinic electroactive colloidal hydrogels for neural tissue engineering applications, Ournal Colloid, Interface Sci. 516 (2018) 57–66.
[4] A. Gevorkian, S.M. Morozova, S. Kheiri, N. Khuu, H. Chen, E. Young, N. Yan, E. Kumacheva, Actuation of three-dimensional-printed nanocolloidal hydrogel with structural anisotropy, Adv. Funct. Mater. 31 (2021) 1–9, https://doi.org/10.1002/adfm.202010743.
[5] E. Prince, Z. Chen, N. Khuu, E. Kumacheva, Nanofibrillar hydrogel recapitulates changes occurring in the fibrotic extracellular matrix, Biomacromolecules. 22 (6) (2021) 2352–2362.
[6] K. Sano, N. Igarashi, Y. Ebina, T. Sasaki, T. Hikima, T. Aida, Y. Ishida, A mechanically adaptive hydrogel with a reconfigurable network consisting entirely of inorganic nanosheets and water, Nat. Commun. 11 (1) (2020).
[7] S.A. Wilson, L.M. Cross, C.W. Peak, A.K. Gaharwar, Shear-Thinning and Thermo-Reversible Nanoengineered Inks for 3D Bioprinting, ACS Appl. Mater. Interfaces. 9 (2017) 43449–43458, https://doi.org/10.1021/acsami.7b13602.
[8] Z. Chen, N. Khuu, F. Xu, S. Kheiri, I. Yakavets, F. Rakhshani, S. Morozova, E. Kumacheva, Printing Structurally Anisotropic Biocompatible Fibrillar Hydrogel for Guided Cell Alignment, Gels. 8 (2022) 685(1–15), https://doi.org/10.3390/gels8110685.
[9] Y. Zhang, Y.u. Wang, H. Wang, Y. Yu, Q. Zhong, Y. Zhao, Super-elastic magnetic structural color hydrogels, Small 15 (35) (2019) 1902198.
[10] J. Tang, J. Sisler, N. Grishkewich, K.C. Tam, Functionalization of cellulose nanocrystals for advanced applications, J. Colloid Interface Sci. 494 (2017) 397–409.
[11] M. Stepanova, E. Korzhikova-Vlakh, Modification of Cellulose Micro- and Nanomaterials to Improve Properties of Aliphatic Polyesters/Cellulose Composites: a review, Polymers (Basel). 14 (2022) 1477, https://doi.org/10.3390/polym14071477.
[12] M. Mariano, N. El Kissi, A. Dufresne, Cellulose nanocrystals and related nanocomposites: Review of some properties and challenges, J. Polym. Sci. Part B Polym. Phys. 52 (2014) 791–806, https://doi.org/10.1002/polb.23490.
[13] G. Siqueira, D. Kokkinis, R. Libanori, M.K. Hausmann, A.S. Gladman, A. Neels, P. Tingaut, T. Zimmermann, J.A. Lewis, A.R. Studart, Cellulose Nanocrystal Inks for 3D, Printing of Textured Cellular Architectures 27 (12) (2017), https://doi.org/10.1002/adfm.201604619.
[14] S. Sultan, G. Siqueira, T. Zimmermann, A.P. Mathew, 3D printing of nano-cellulosic biomaterials for medical applications, Curr. Opin. Biomed. Eng. 2 (2017) 29–34.
[15] Q. Wang, J. Sun, Q. Yao, C. Ji, J. Liu, Q. Zhu, 3D printing with cellulose materials, Cellulose. 25 (2018) 4275–4301, https://doi.org/10.1007/s10570-018-1888-y.
[16] S. Uman, A. Dhand, J.A. Burdick, Recent advances in shear-thinning and self-healing hydrogels for biomedical applications, J. Appl. Polym. Sci. 137 (25) (2020), https://doi.org/10.1002/app.48668.
[17] M. Chau, S.E. Sriskandha, D. Pichugin, H. Thérien-Aubin, D. Nykypanchuk, G. Chauve, M. Méthot, J. Bouchard, O. Gang, E. Kumacheva, Ion-Mediated Gelation of Aqueous Suspensions of Cellulose Nanocrystals, Biomacromolecules. 16 (2015) 2455–2462, https://doi.org/10.1021/acs.biomac.5b00701.
[18] A. Khabibullin, M. Alizadehgiashi, N. Khuu, E. Prince, M. Tebbe, E. Kumacheva, Injectable shear-thinning fluorescent hydrogel formed by cellulose nanocrystals and graphene quantum dots, Langmuir. 33 (2017) 12344–12350, https://doi.org/10.1021/acs.langmuir.7b02906.
[19] J.H.L. da Fonsêca, M.A. d'Ávila, Rheological behavior of carboxymethylcellulose and cellulose nanocrystal aqueous dispersions, Rheol. Acta. 60 (9) (2021) 497–509.
[20] B. Peng, J. Tang, P. Wang, J. Luo, P. Xiao, Y. Lin, K.C. Tam, Rheological properties of cellulose nanocrystal-polymeric systems, Cellulose. 25 (6) (2018) 3229–3240.
[21] Y. Li, N. Khuu, A. Gevorkian, S. Sarjinsky, H. Therien-Aubin, Y. Wang, S. Cho, E. Kumacheva, Supramolecular Nanofibrillar Thermoreversible Hydrogel for Growth and Release of Cancer Spheroids, Supramolecular Nanofibrillar Thermoreversible Hydrogel for Growth and Release of Cancer Spheroids 56 (22) (2017) 6083–6087.
[22] E. Gicquel, C. Martin, L. Heux, B. Jean, J. Bras, Adsorption versus grafting of poly (N-Isopropylacrylamide) in aqueous conditions on the surface of cellulose nanocrystals, Carbohydr. Polym. 210 (2019) 100–109, https://doi.org/10.1016/j.carbpol.2019.01.022.
[23] J. Shang, P. Theato, Smart composite hydrogel with pH-, ionic strength- and temperature-induced actuation, Soft Matter. 14 (2018) 8401–8407, https://doi.org/10.1039/c8sm01728j.
[24] L. Tang, L. Wang, X. Yang, Y. Feng, Y.u. Li, W. Feng, Poly (N-isopropylacrylamide)-based smart hydrogels: design, properties and applications, Prog. Mater. Sci. 115 (2021), https://doi.org/10.1016/j.pmatsci.2020.100702.
[25] M.L. Ohnsorg, J.M. Ting, S.D. Jones, S. Jung, F.S. Bates, T.M. Reineke, Tuning PNIPAm self-assembly and thermoresponse: roles of hydrophobic end-groups and hydrophilic comonomer, Polym. Chem. 10 (2019) 3469–3479, https://doi.org/10.1039/C9PY00180H.
[26] M, Rubinstein, R.H, Colby, Polymer Physics, (n.d.).
[27] K. Kubota, K. Hamano, N. Kuwahara, S. Fujishige, I. Ando, Characterization of poly (N-isopropylmethacrylamide) in water, Polym. J. 22 (12) (1990) 1051–1057.
[28] M.J, Lang, X, Patrick, A. D, Hammouda, B, Hore, Chain terminal group leads to distinct thermoresponsive behaviors of linear PNIPAM and polymer analogs, Polmer. 145 (2018) 137–147.
[29] S, Wu, C, Zhou, Thermodynamically stable globule state of a single poly (N-isopropylacrylamide) chain in water, Macromolecules. 28 (1995) 5388–5390.
[30] M. Stepanova, A. Dobrodumov, I. Averianov, I. Gofman, J. Nashchekina, I. Guryanov, I. Klyukin, A. Zhdanov, E. Korzhikova-Vlakh, K. Zhizhin, Design, fabrication and characterization of biodegradable composites containing closo-borates as potential materials for boron neutron capture therapy, Polymers (Basel). 14 (2022) 3864, https://doi.org/10.3390/polym14183864.
[31] F. Sciortino, P. Tartaglia, E. Zaccarelli, One-dimensional cluster growth and branching gels in colloidal systems with short-range depletion attraction and screened electrostatic repulsion, J. Phys. Chem. B. 109 (46) (2005) 21942–21953.
[32] C.J. Dibble, M. Kogan, M.J. Solomon, Structure and dynamics of colloidal depletion gels: coincidence of transitions and heterogeneity, Phys. Rev. E. 74 (4) (2006) 041403.
[33] S.M. Ilett, A. Orrock, W.C.K. Poon, P.N. Pusey, Phase behavior of a model colloid-polymer mixture, Phys. Rev. E. 51 (2) (1995) 1344–1352.
[34] C.A. Saez Cabezas, G.K. Ong, R.B. Jadrich, B.A. Lindquist, A. Agrawal, T.M. Truskett, D.J. Milliron, Gelation of plasmonic metal oxide nanocrystals by polymer-induced depletion attractions, Proc. Natl. Acad. Sci. 115 (36) (2018) 8925–8930.
[35] J. Luo, G. Yuan, C. Zhao, C.C. Han, J. Chen, Y. Liu, Soft Matter Gelation of large hard particles with short-range attraction induced by bridging of small soft microgels, Soft Matter. 11 (12) (2015) 2494–2503.
[36] A. You, M.A.Y. Be, I. In, On Interaction between Two Bodies Immersed in a Solution of Macromolecules, J. Chem. Phys. 1255 (1954) 1–3.
[37] H. Kojima, Studies on the phase transition of hydrogels and aqueous solutions of thermosensitive polymers, Polym. J. 50 (2018) 411–418, https://doi.org/10.1038/s41428-018-0035-9.
[38] A. Halperin, M. Kröger, F.M. Winnik, Poly(N -isopropylacrylamide) phase diagrams: fifty years of research, Angew. Chemie Int. Ed. 54 (2015) 15342–15367, https://doi.org/10.1002/anie.201506663.
[39] T. Trongsatitkul, B.M. Budhlall, Microgels or microcapsules? Role of morphology on the release kinetics of thermoresponsive PNIPAm-co-PEGMa hydrogels, Polym. Chem. 4 (2013) 1502–1516, https://doi.org/10.1039/C2PY20889J.
[40] H. Feil, Y.H. Bae, J. Feijen, S.W. Kim, Effect of comonomer hydrophilicity and ionization on the lower critical solution temperature of N-isopropylacrylamide copolymers, Macromolecules. 26 (1993) 2496–2500, https://doi.org/10.1021/ma00062a016.
[41] R. Francis, C.P. Jijil, C.A. Prabhu, C.H. Suresh, Synthesis of poly(N-isopropylacrylamide) copolymer containing anhydride and imide comonomers – a theoretical study on reversal of LCST, Polymer (Guildf). 48 (2007) 6707–6718, https://doi.org/10.1016/j.polymer.2007.08.061.
[42] W. Qi, J. Yu, Z. Zhang, H.-N. Xu, Effect of pH on the aggregation behavior of cellulose nanocrystals in aqueous medium, Mater. Res. Express. 6 (2019), https://doi.org/10.1088/2053-1591/ab5974 125078.
[43] B.M. Anikushin, P.G. Lagutin, A.M. Kanbetova, A.A. Novikov, V.A. Vinokurov, Zeta potential of nanosized particles of cellulose as a function of pH, Chem. Technol. Fuels Oils. 57 (2022) 913–916, https://doi.org/10.1007/s10553-022-01328-0.
[44] R.H. Smellie, V.K. La Mer, Flocculation, subsidence and filtration of phosphate slimes: VI. a quantitative theory of filtration of flocculated suspensions, J. Colloid Sci. 599 (1958) 589–599.
[45] J.H.L. da Fonsêca, M.A. D'Ávila, Rheological behavior of carboxymethylcellulose and cellulose nanocrystal aqueous dispersions, Rheol. Acta. 60 (2021) 497–509, https://doi.org/10.1007/s00397-021-01292-2.
[46] B. Peng, J. Tang, P. Wang, J. Luo, P. Xiao, Y. Lin, K.C. Tam, Rheological properties of cellulose nanocrystal-polymeric systems, Cellulose. 25 (2018) 3229–3240, https://doi.org/10.1007/s10570-018-1775-6.
[47] H. Thérien-Aubin, Y. Wang, K. Nothdurft, E. Prince, S. Cho, E. Kumacheva, Temperature-responsive nanofibrillar hydrogels for cell encapsulation, Biomacromolecules. 17 (10) (2016) 3244–3251.
[48] L. Geurds, J. Lauko, A.E. Rowan, N. Amiralian, Tailored nanocellulose-grafted polymer brush applications, J. Mater. Chem. A. 9 (32) (2021) 17173–17188.
[49] B.M, Trongsatitkul, T, Budhlall, Microgels or Microcapsules? Role of Morphology on the Release Kinetics of Thermoresponsive PNIPAm-co-PEGMA Hydrogels, Polym. Chem. 4 (2013) 1502–1516.
[50] Q, He, X, Lu, Design and fabrication strategies of cellulose nanocrystal-based hydrogel and its highlighted application using 3D printing: A review, Carbohydr. Polym. 2022 120351. https://doi.org/10.1016/j.carbpol.2022.120351.